Supporting Information

POM-based porous supramolecular framework for the efficient sulfide-sulfoxide transformation with low molar O/S ratio

Yanhong Chen, Haiyan An,* Shenzhen Chang, Yanqin Li, Qingshan Zhu, Huiyun Luo, Yaohui Huang

State Key Laboratory of Fine Chemicals, School of Chemical Engineering, Dalian University of Technology, Dalian 116023, People's Republic of China

*Corresponding author. Tel: +86-411-84657675. E-mail address: anhy@dlut.edu.cn

CONTENTS:

Section I. Supplementary experimental section

Section II. Supplementary structure figures

Section III. Supplementary physical characterizations

Section IV. Supplementary tables

Section V. References

Section I. Supplementary experimental section

1.1 Materials and instrumentation.

2-(pyridinium-4-yl)-1H-imidazole-4,5-dicarboxylic acid was synthesized based on the literature method,[1,2] which can be proved by IR spectra. Other reagents and solvents were used as received from commercial suppliers without further purification. 1H NMR spectra were recorded on a Bruker DRX spectrometer operating at 400 MHz. Elemental analyses (H, C and N) were performed on a Perkin-Elmer 2400 CHN elemental analyzer. IR spectra were recorded in the range 4000-400 cm^{-1} on a Nexus Euro FT/IR Spectrophotometer using KBr pellets. The powder X-ray diffraction (PXRD) patterns of the as-prepared products were carried out by using Rigaku Smart Lab X-ray diffractometer with Cu-Kα radiation (λ = 0.154 nm) and 2θ transforming from 5 to 50°. The X-ray single crystal diffraction of the as-prepared products were collected by Bruker D8 Venture single crystal diffractometer with Mo-Kα radiation. Liquid UV-vis spectra were measured from 200 to 800 nm on Techcomp UV1000 spectrophotometer. The products in catalytic experiments were determined by gas chromatography with SE-54 capillary column (Techcomp GC 7900II) and gas chromatography-mass spectroscopy (Trace ISQ).

1.2 X-Ray crystallography.

The crystal data of **1** and **2** were collected at 295(2) K and 150(2) K with graphite monochromatic Mo Kα radiation (λ = 0.71073 Å). The crystal structures were solved and refined by full matrix least-squares methods against F^2 by using SHELXTL-2018 programs.[3,4] All non-hydrogen atoms were refined with anisotropic temperature parameters. All hydrogen atoms associated with C and N atoms were placed in geometrically idealized positions using a riding model. For compound **1**, the contribution of partial solvent electron densities was removed by the SQUEEZE routine in PLATON program.[5] Crystallographic data, structure refinements and CCDC reference numbers for **1** and **2** are listed in Table S1.

1.3 Calculations of efficiency of hydrogen peroxide in the sulfoxidation reaction system.

The reaction mixture was vigorously stirred under preset conditions, and was quickly filtered with a syringe filter to remove the catalysts. The residual H_2O_2 concentration of the supernatant was determined by titration with 0.002 M $Ce(NH_4)_2(NO_3)_6$ solution. The titration indicator, Ferroin (0.025 $mol\cdot L^{-1}$), was prepared with 1,10-phenanthroline and $FeSO_4\cdot 7H_2O$ based on a 3:1 stoichiometric relationship. And according to the color of the mixture solution from nacarat to blue the titration end-point was determined.

- The H_2O_2 utilization efficiency was calculated according to the following formula (Assuming that one mol of oxidant reacts with one mol of substrate):

$$\mathbf{H_2O_2\ efficiency\ (\%) = 100\ x\ \frac{mol\ of\ H_2O_2\ consumed\ in\ the\ formation\ of\ sulfoxides}{mol\ of\ H_2O_2\ converted}}$$

- Part I: The calculations are shown with oxidation of methyl phenyl sulfide (MPS) to methyl phenyl sulfoxide (MPSO), with catalysts **1** and **2**.

  ✧ *For catalyst **1***: (i) H_2O_2 (mmol) consumed in the formation of sulfoxide (yield: >99%) from 0.25 mmol sulfides = **0.25 mmol**. (ii) The titrated value was found to be: 0.02304 mmol. Since 0.30 mmol H_2O_2 has been originally used for the reaction. Therefore, total mol of H_2O_2 converted = (0.30-0.02304) mmol = **0.27696 mmol**. Thus, H_2O_2 efficiency = 100 × [0.25/0.27696] = **90.3%**.

  ✧ *For catalyst **2***: (i) H_2O_2 (mmol) consumed in the formation of sulfoxide (yield: >99%) from 0.25 mmol sulfides = **0.25 mmol**. (ii)The titrated value was found to be: 0.02056 mmol. Since 0.30 mmol H_2O_2 has been originally used for the reaction. Therefore, total mol of H_2O_2 converted = (0.30-0.02056) mmol =

0.27944 mmol. Thus, H_2O_2 efficiency = 100 × [0.25/0.27944] = **89.5%**

- Part II: The calculations are shown with oxidation of 2-chloroethyl ethyl sulfide (CEES) to 2-chloroethyl ethyl sulfoxide (CEESO), with catalysts **1** and **2**.

  ✧ *For catalyst **1***: (i) H_2O_2 (mmol) consumed in the formation of CEESO (yield: >99%) from 0.25 mmol CEES = **0.25 mmol**. (ii) The titrated value was found to be: 0.03552 mmol. Since 0.30 mmol H_2O_2 has been originally used for the reaction. Therefore, total mol of H_2O_2 converted = (0.30-0.03552) mmol = **0.26448 mmol** Thus, H_2O_2 efficiency = 100 × [0.25/0.26448] = **94.5%**

  ✧ *For catalyst **2***: (i) H_2O_2 (mmol) consumed in the formation of CEESO (yield: >99%) from 0.25 mmol CEES = **0.25 mmol**. (ii) The titrated value was found to be: 0.03022 mmol. Since 0.30 mmol H_2O_2 has been originally used for the reaction. Therefore, total mol of H_2O_2 converted = (0.30-0.03022) mmol = **0.26978 mmol**. Thus, H_2O_2 efficiency = 100 × [0.25/0.26978] = **92.7%**.

Section II. Supplementary structure figures

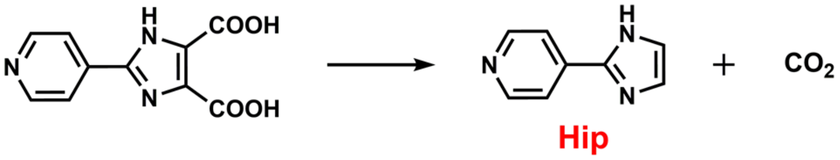

Scheme S1. Schematic diagram of ligands conversion in-situ.

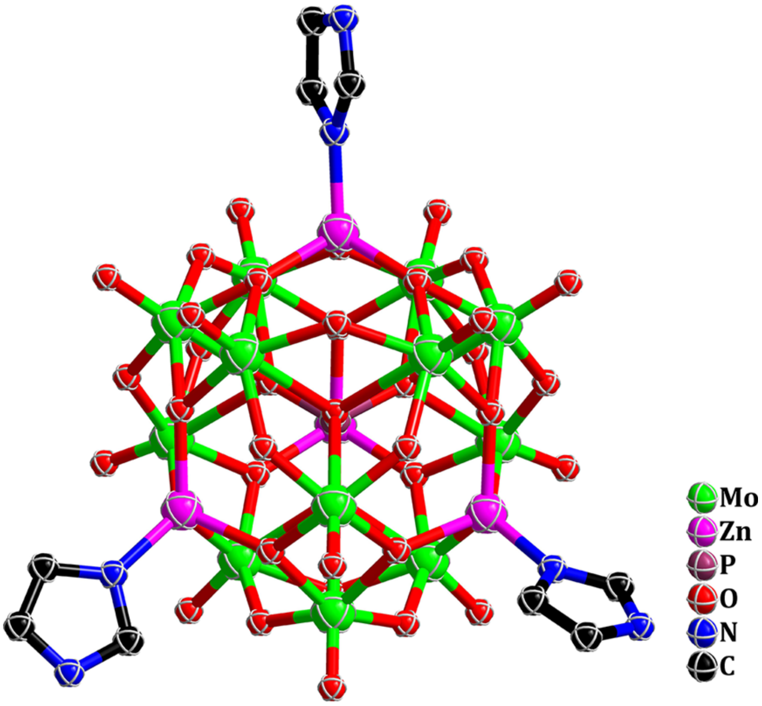

Fig. S1. Asymmetric unit of compound **1**.
Counter cations and hydrogen atoms are omitted for clarity.

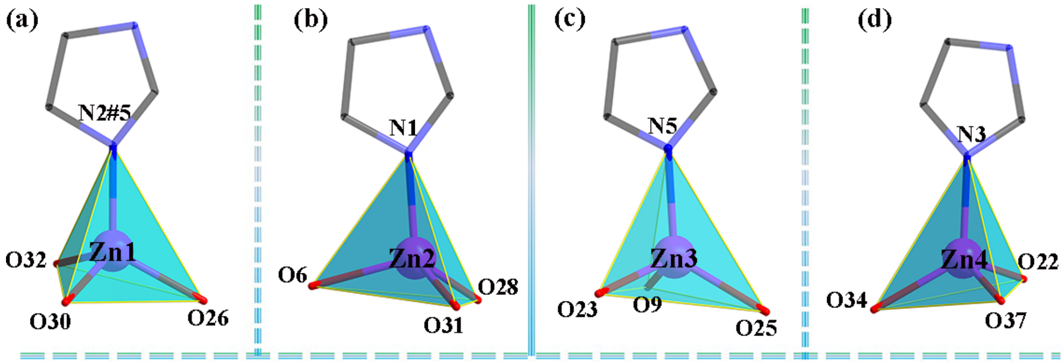

Fig. S2. The coordination modes of Zn ions in compound **1**.
(a) Zn1, (b) Zn2, (c) Zn3 and (d) Zn4. Symmetry transformations used to generate equivalent atoms: #5: 1/4-y, 3/4+x, -1/4+z.

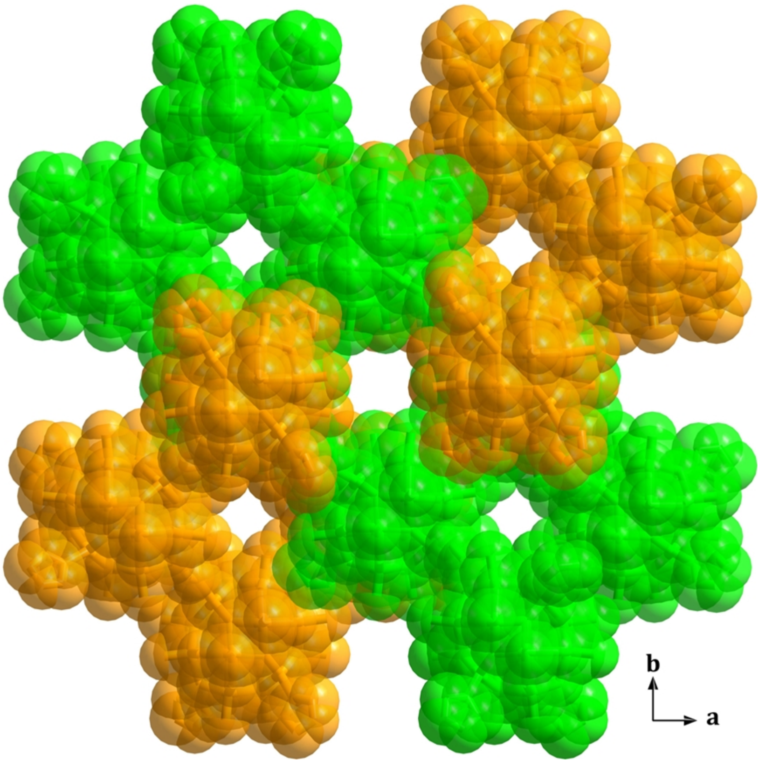

Fig. S3. The 3D space-filling framework of compound **1**.

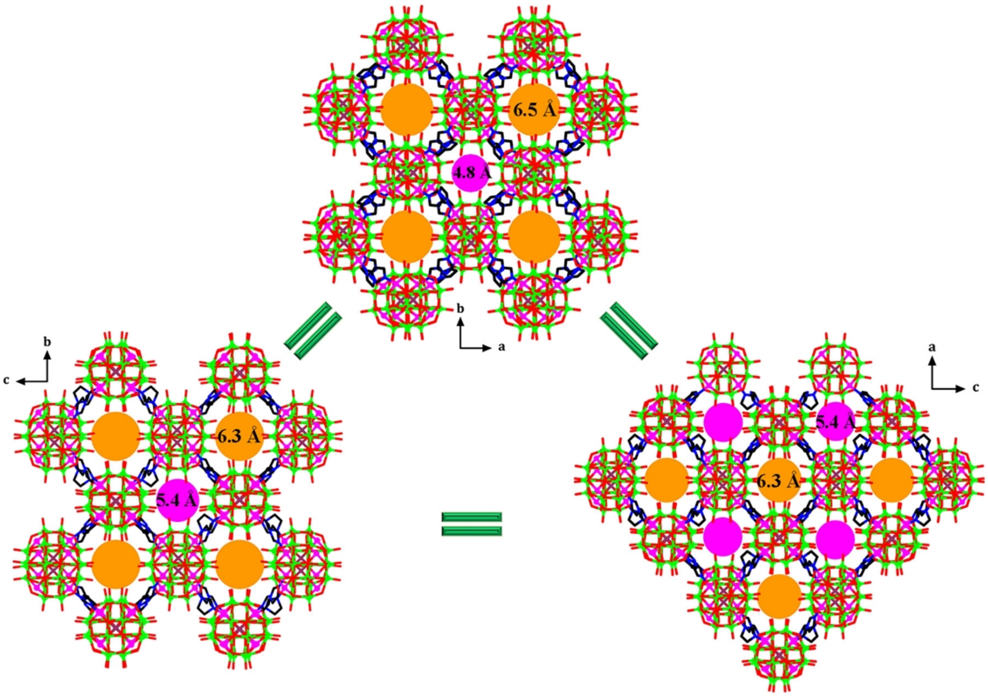

Fig. S4. Porous framework viewed from different directions in compound **1**.
TOP: viewed from c-axis. *Bottom left*: viewed from a-axis. *Bottom right*: viewed from b-axis.

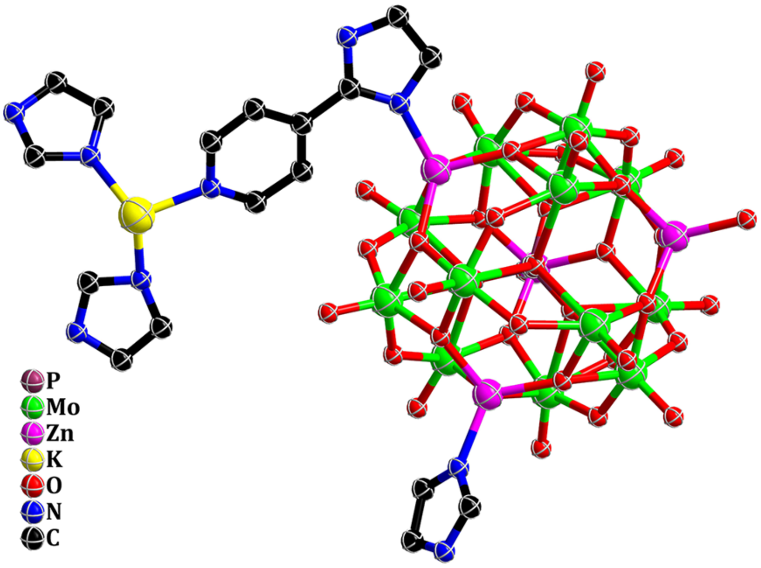

Fig. S5. Asymmetric unit of compound **2**.
Counter cations and hydrogen atoms are omitted for clarity.

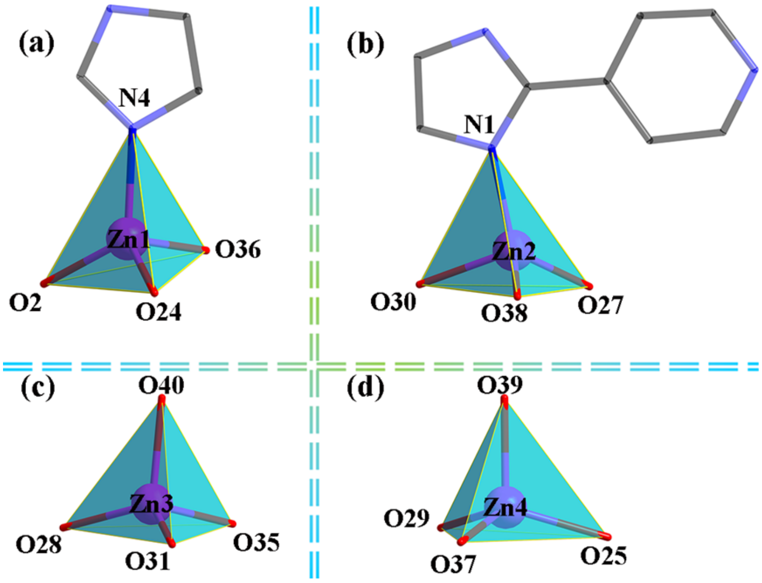

Fig. S6. The coordination modes of Zn ions in compound **2**.
(a) Zn1, (b) Zn2, (c) Zn3 and (d) Zn4.

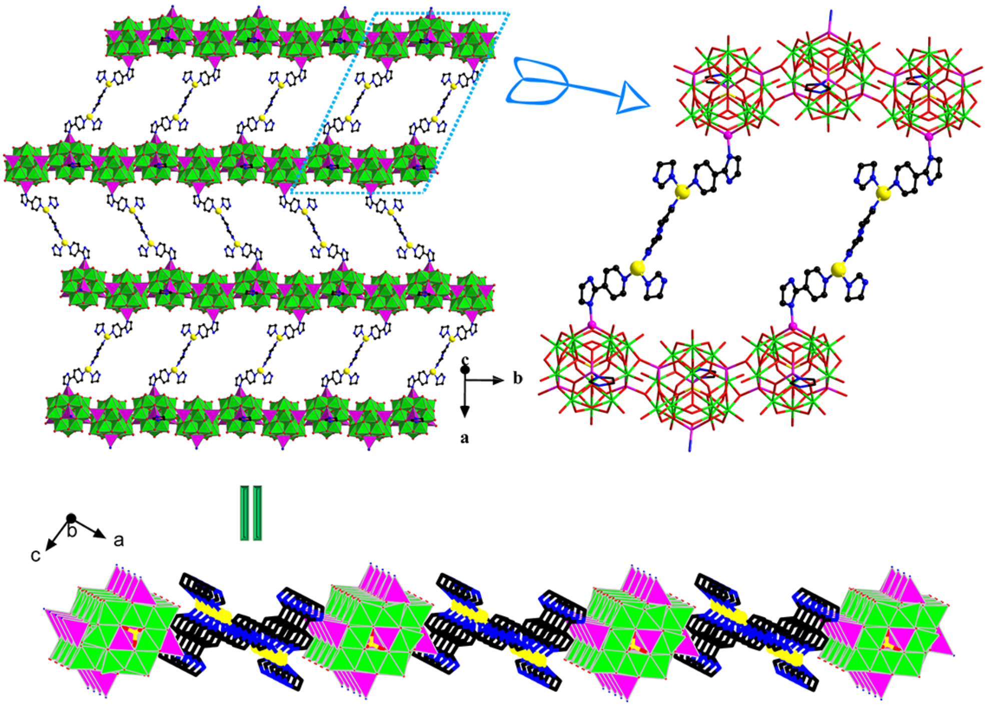

Fig. S7. 2D layer of compound **2**.
TOP: viewed from c-axis. *Bottom*: viewed from b-axis.

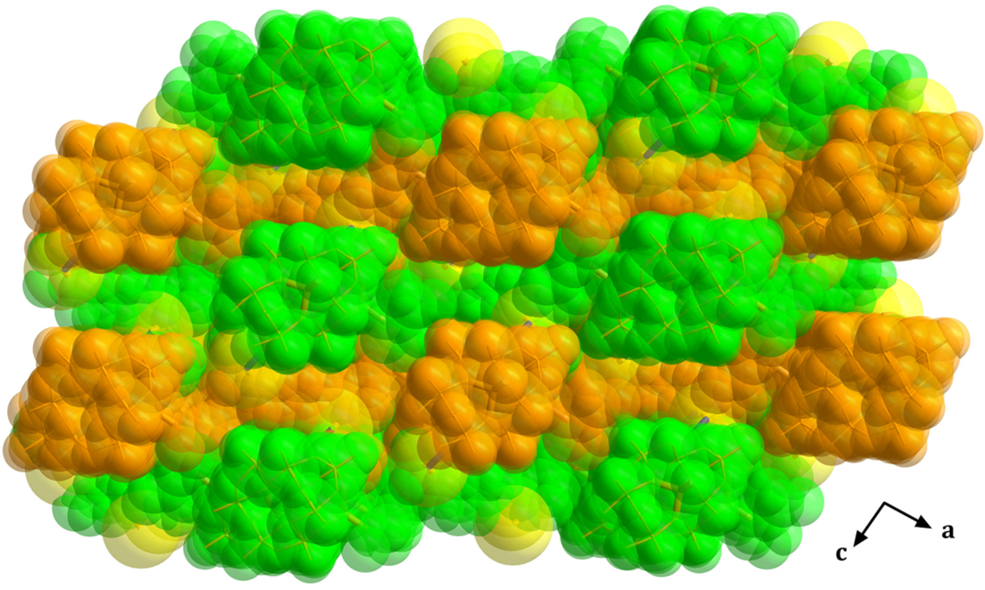

Fig. S8. The 3D space-filling framework of compound **2**.

Section III. Supplementary physical characterizations

IR spectra of **1** and **2** are shown in Fig. S9, the signatures of P−O, Mo=O and Mo−O−Mo vibrations of the inorganic skeleton of the ε-Keggin POM are around 1070 cm^{-1}, 965 cm^{-1}, 935 cm^{-1}, 903 cm^{-1}, 815 and 784 cm^{-1}, respectively. Obviously, in the high-wavenumber region (v > 1100 cm^{-1}), the signatures of C=C, C=N, C−H and N−H vibrations of the organic ligand are around 1140−1622 cm^{-1} and 2870−3571 cm^{-1}.

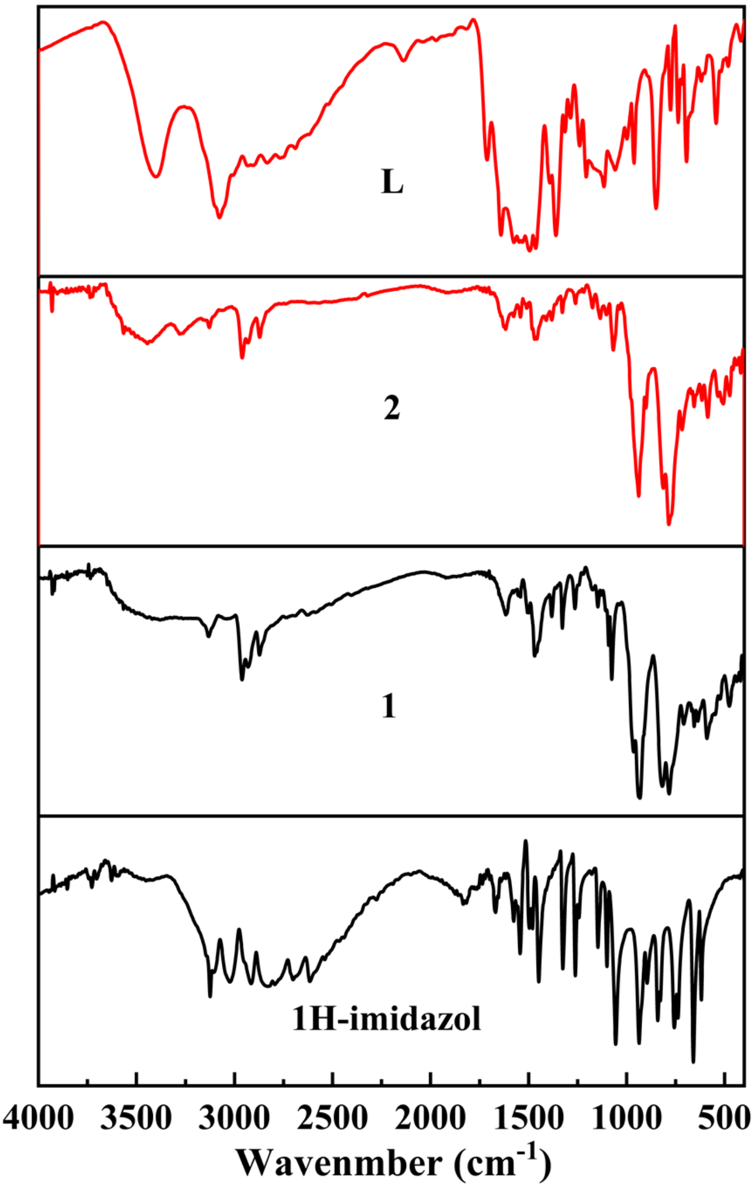

Fig. S9. IR spectra for **1**, **2**, and Ligands.
L: 2-(pyridinium-4-yl)-1H-imidazole-4,5-dicarboxylic acid.

The measured powder X-ray diffraction (PXRD) spectra of **1** and **2** are consistent with the simulated XRD spectra of X-ray structure analysis, indicating that they have good phase purity. (Fig. S10).

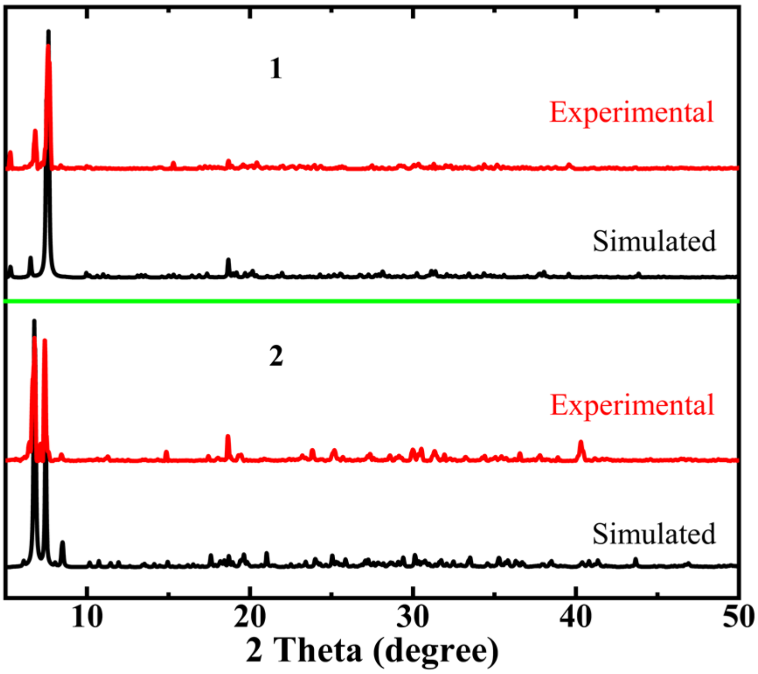

Fig. S10. Experimental and simulated powder X-ray diffraction patterns of **1** and **2**.

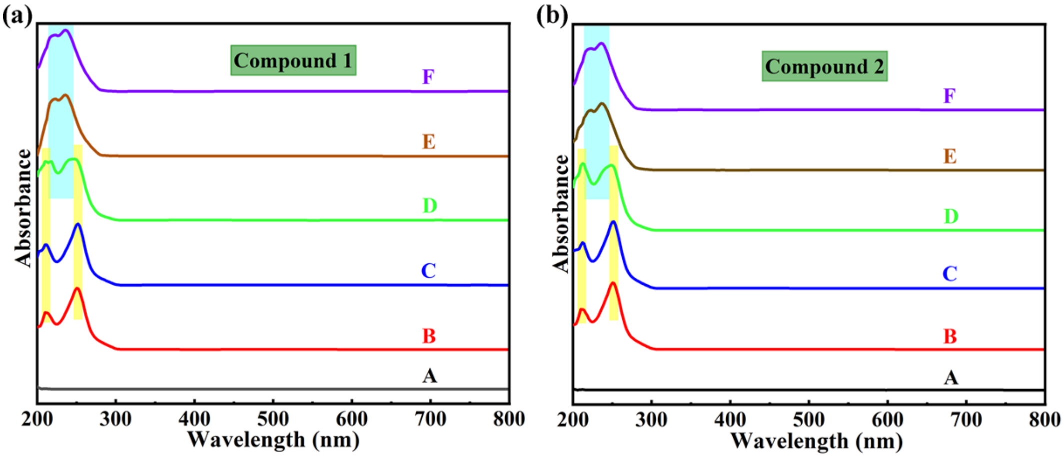

Fig. S11. The UV-vis spectra of MPS oxidation catalyzed by **1** and **2**.

(A) the UV-vis spectra of filtrate after reaction for 10-15 min under the optimal conditions without substrate; (B) the UV-vis spectra of pure MPS; (C) the UV-vis spectra of filtrate before reaction; (D) the UV-vis spectra of filtrate after reaction 3 min for **1** and 5 min for **2**; (E) the UV-vis spectra of filtrate after reaction 10 min for **1** and 15 min for **2**; (F) the UV-vis spectra of pure MPSO.

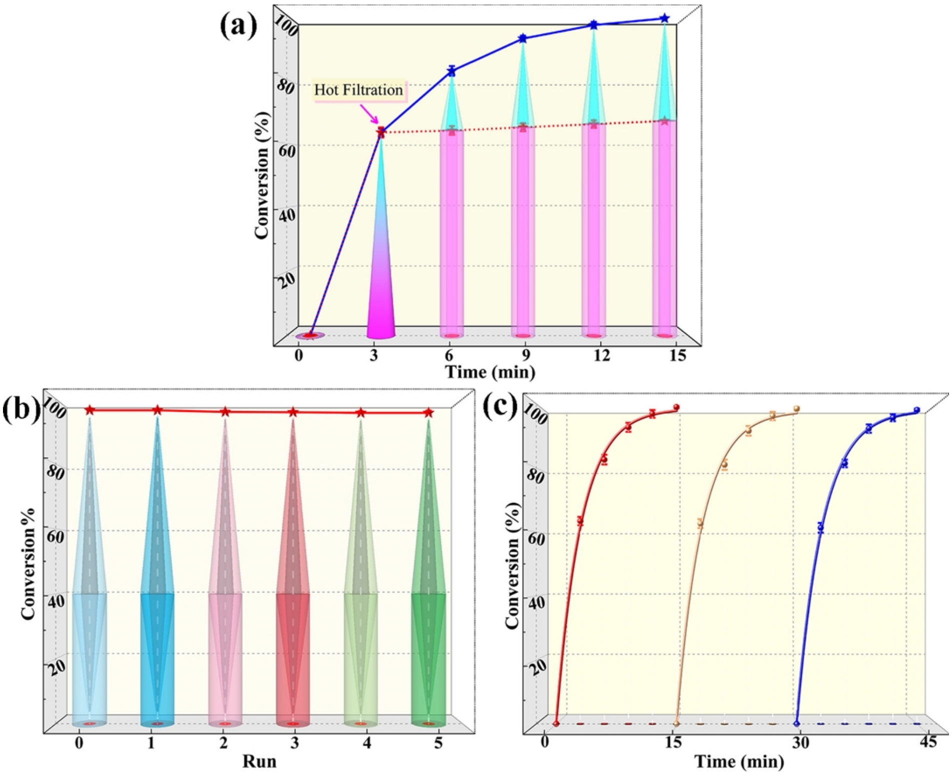

Fig. S12. Hot filtration and catalytic activity stability experiment of **2** in MPS oxidation.

(a) Hot filtration experiment for MPS oxidation over **2**. (b) The recycle test of the oxidation of MPS was carried out with the recovered **2**. (c) The continuous recycle test for the oxidation of MPS using **2**.

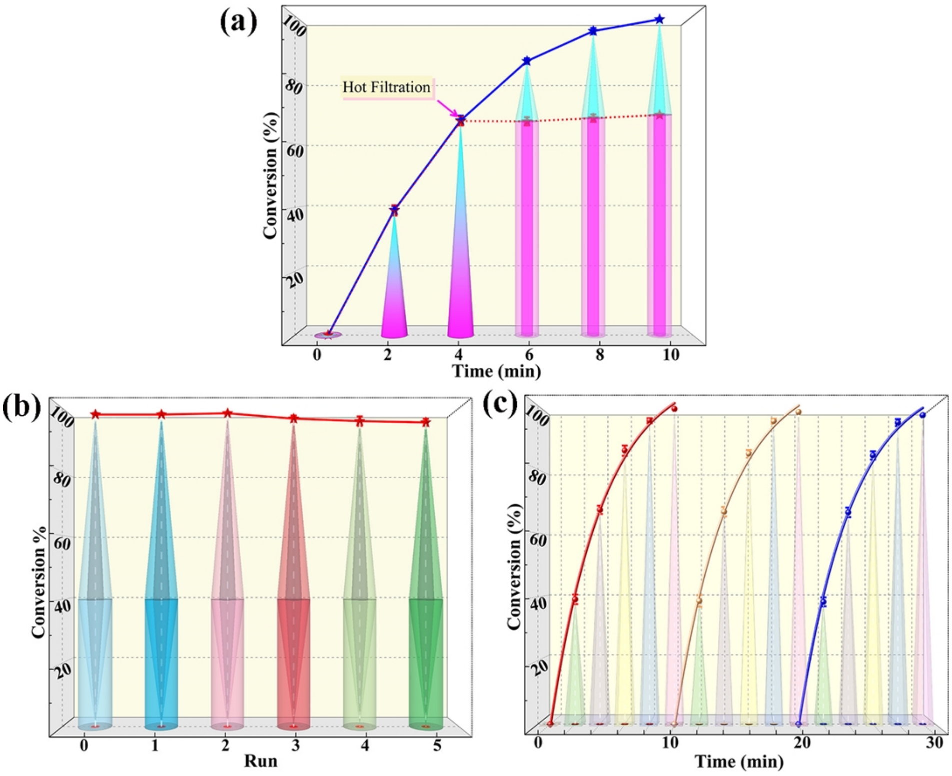

Fig. S13. Hot filtration and catalytic activity stability experiment of **1** in CEES oxidation.

(a) Hot filtration experiment for CEES oxidation over **1**. (b) The recycle test of the oxidation of CEES was carried out with the recovered **1**. (c) The continuous recycle test for the oxidation of CEES using **1**.

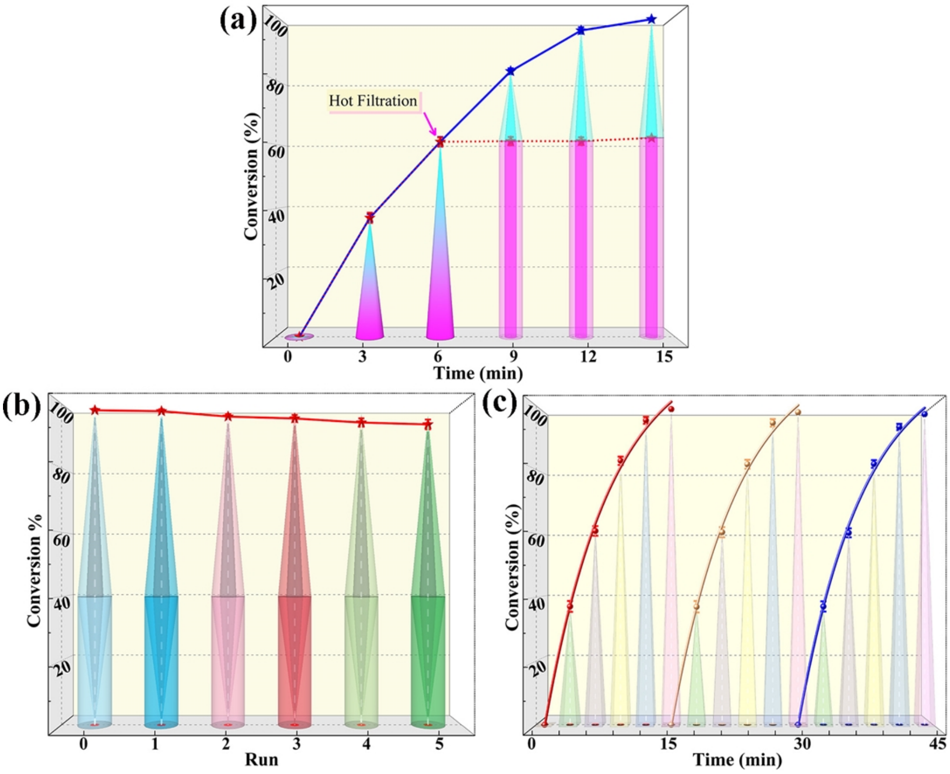

Fig. S14. Hot filtration and catalytic activity stability experiment of **2** in CEES oxidation.
(a) Hot filtration experiment for CEES oxidation over **2**. (b) The recycle test of the oxidation of CEES was carried out with the recovered **2**. (c) The continuous recycle test for the oxidation of CEES using **2**.

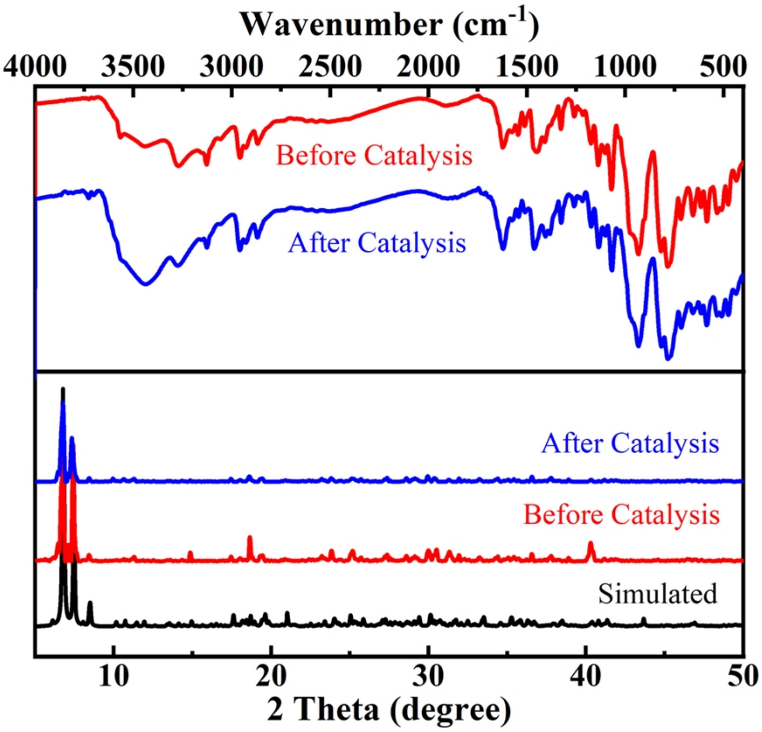

Fig. S15. The IR spectra and PXRD patterns of fresh and spent **2**.

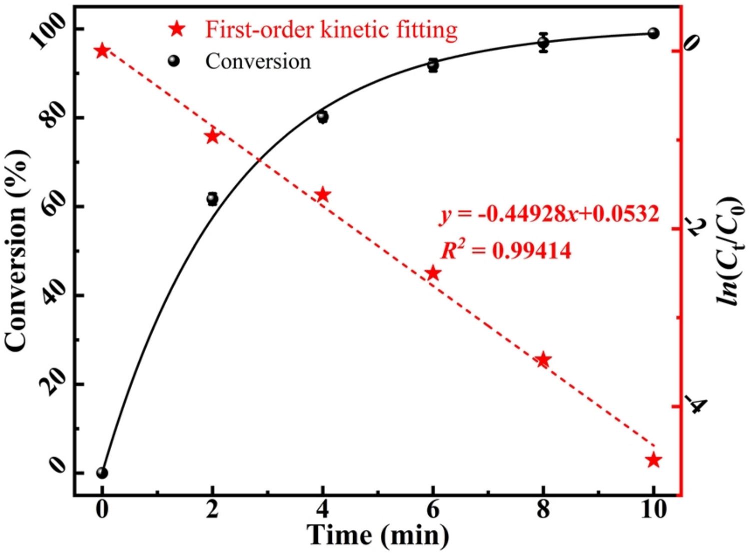

Fig. S16. Kinetic profiles of oxidation of MPS catalyzed by **1** at 50 °C.

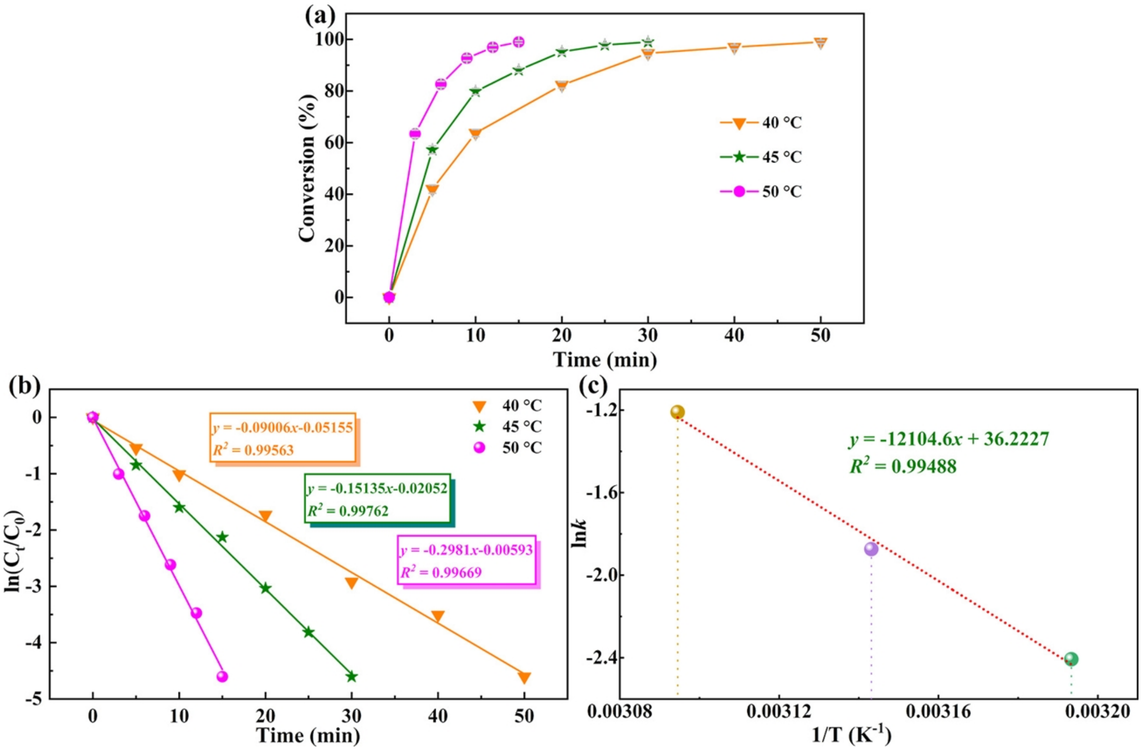

Fig. S17. Kinetic analysis of the oxidation of MPS catalyzed **2**.

(a) The kinetic profiles of the oxidation of MPS catalyzed by compound **1** at 40 °C, 45 °C and 50 °C. (b) The Arrhenius−Eyring plot (*lnk = –(Ea/RT) + lnA*).

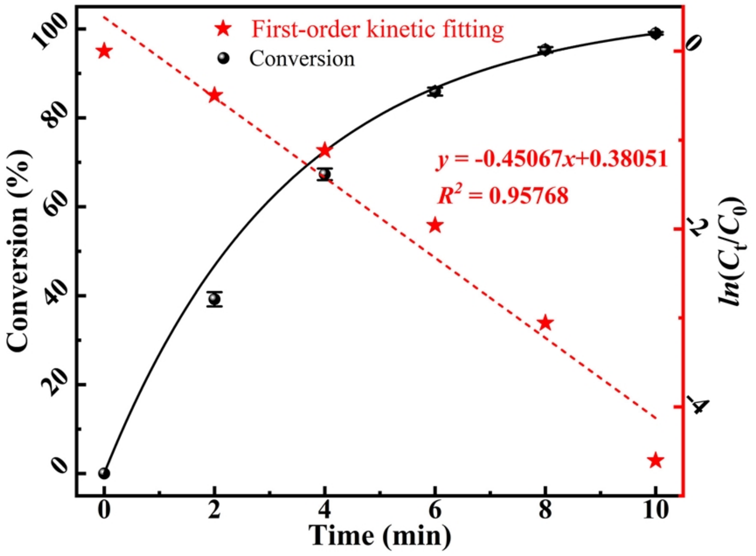

Fig. S18. Kinetic profiles of oxidation of CEES catalyzed by **1** at room temperature.

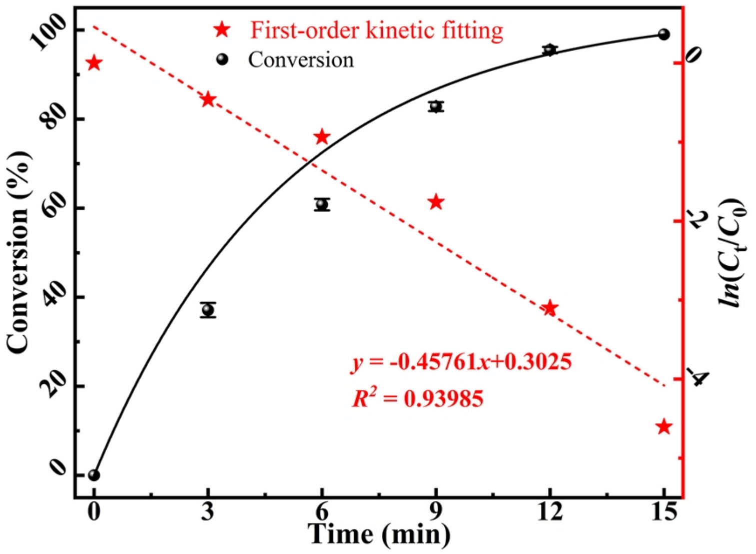

Fig. S19. Kinetic profiles of oxidation of CEES catalyzed by **2** at room temperature.

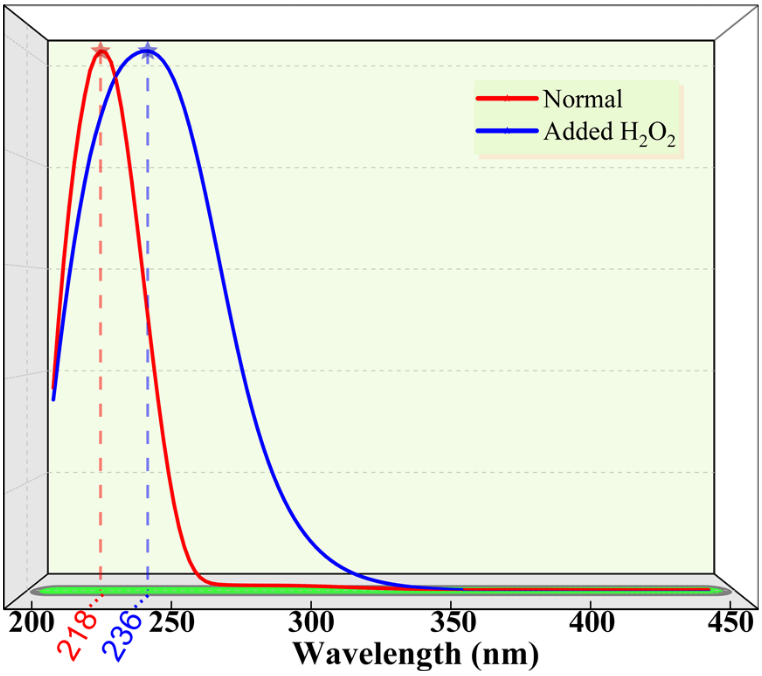

Fig. S20. UV-vis spectra of **2** before and after treatment with H_2O_2.

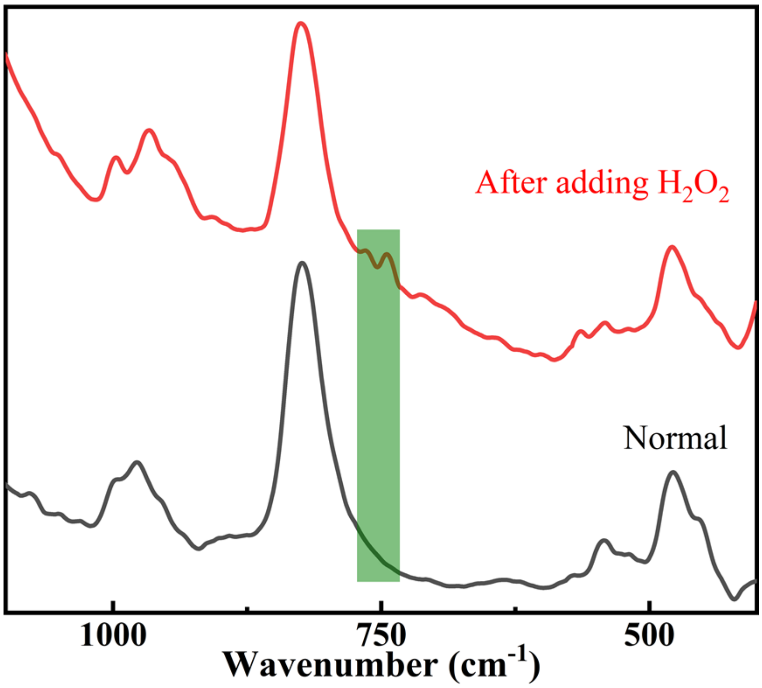

Fig. S21. Raman spectra of **1** before and after treatment with H_2O_2.

Section IV. Supplementary tables

Table S1. Crystal data and structure refinement for **1** and **2**.

	Compound **1**	Compound **2**
CCDC number	2120945	2120946
Formula	$C_{41}H_{89}Mo_{12}N_8O_{42}PZn_4$	$C_{33}H_{56}KMo_{12}N_{10}O_{40}PZn_4$
Formula weight	2809.93	2715.70
T (K)	295(2) K	150(2) K
Crystal system	Tetragonal	Monoclinic
Space group	$I4_1/a$	$P2_1/n$
a (Å)	33.2771(7)	14.2512(4)
b (Å)	33.2771(7)	17.3920(4)
c (Å)	32.1701(11)	26.0369(7)
α (°)	90	90
β (°)	90	96.7360(10)
γ (°)	90	90
V (Å^3)	35624.1(19)	6408.9(3)
Z	16	4
μ (mm^{-1})	2.780	3.920
Index ranges	-39<=h<=39 -39<=k<=34 -37<=l<=38	-16<=h<=16 -20<=k<=20 -30<=l<=30
Reflections collected	104422	46781
Independent reflections	15677	11261
R_{int}	0.1029	0.0678
Data/restraints/parameters	15677/50/797	11261/574/911
GOF on F^2	1.036	1.033
R_1, wR_2 [$I > 2\sigma(I)$]	0.0888, 0.1932	0.0405, 0.0946
R_1, wR_2 (all data)	0.1242, 0.2042	0.0705, 0.1066

$R_1 = \Sigma||F_o| - |F_c||/\Sigma|F_o|$. $wR_2 = \Sigma[w(F_o^2 - F_c2)^2]/\Sigma[w(F_o^2)^2]^{1/2}$

Table S2. The BVS calculations of Mo, P and Zn and selected bonds for **1** and **2**.

Code	Compound **1**			Compound **2**		
	BVS	**Selected bond**	**Bond lengths (Å)**	**BVS**	**Selected bond**	**Bond lengths (Å)**
Mo1	5.29			5.41		
Mo2	5.33	**Mo(1)-Mo(12)**	2.6324(19)	6.01	**Mo(1)-Mo(10)**	2.6222(10)
Mo3	5.27			6.12		
Mo4	6.02			5.33		
Mo5	5.22	**Mo(2)-Mo(6)**	2.639(2)	5.20	**Mo(2)-Mo(8)**	3.1814(9)
Mo6	5.45			6.04		
Mo7	6.18			5.37		
Mo8	6.06	**Mo(3)-Mo(11)**	2.6368(19)	6.04	**Mo(3)-Mo(6)**	3.1949(9)
Mo9	5.33			5.31		
Mo10	6.12			5.28		
Mo11	5.42	**Mo(4)-Mo(10)**	3.1817(18)	5.24	**Mo(4)-Mo(5)**	2.6361(11)
Mo12	5.38			5.25		
P1	4.70			4.78		
Zn1	2.02	**Mo(5)-Mo(9)**	2.629(2)	2.00	**Mo(7)-Mo(12)**	2.6238(11)
Zn2	2.03			1.98		
Zn3	2.03	**Mo(7)-Mo(8)**	3.174(2)	1.98	**Mo(9)-Mo(10)**	2.6077(10)
Zn4	2.00			1.97		

Table S3. The molecular sizes of MPS, CEES, and their oxidation products[a].

MPS (↓)	MPSO (↓)	$MPSO_2$ (↓)
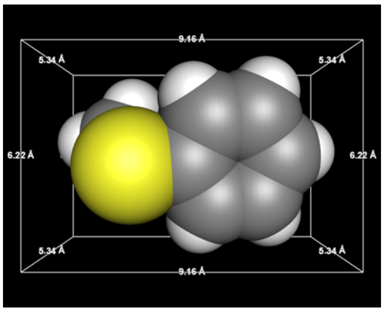	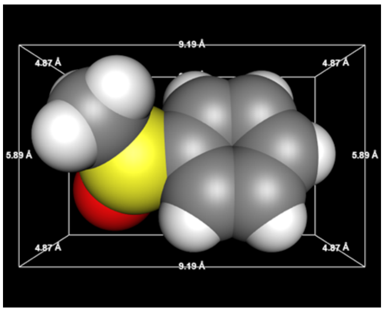	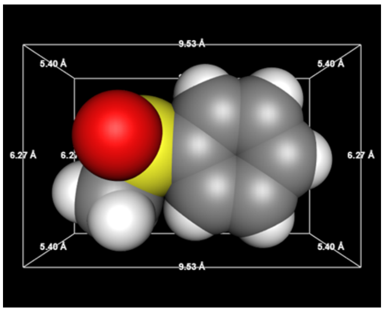
CEES (↓)	CEESO (↓)	$CEESO_2$ (↓)
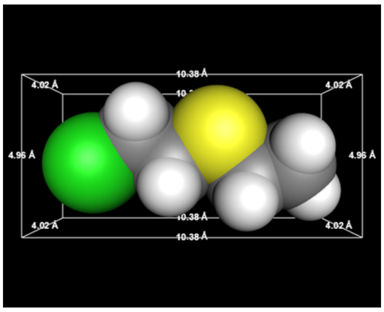	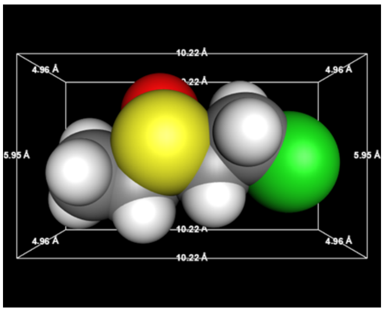	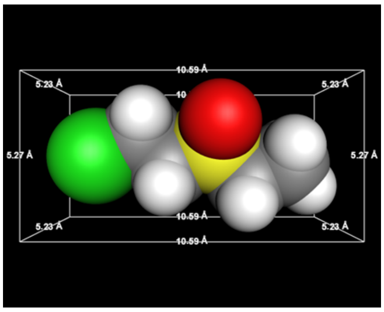

[a] These molecular sizes are calculated based on the Corey-Pauling-Koltun (CPK) model.

Table S4. Summary of the MPS oxidation over different catalyst systems.

catal.	oxid.	O/S[a]	temp. (°C)	time (min)	conv. (%)	sel. (%)[c]	TOF (h^{-1})[b]	ref.
Catalyst 1	H_2O_2	1.2	50	10	>99	>99	1200	—[c]
Catalyst 2	H_2O_2	1.2	50	15	>99	>99	800	—[c]
Mo_{132}	H_2O_2	2	rt	45	100	100	13333.3	6
Mo_{132}	H_2O_2	2	rt	45	100	100[d]	666.7	6
$Cu_8(Mo_8)_2$	TBHP	1.6	50	30	99	99	198	7
$Tb_3(Mo_8)_2$	H_2O_2	2	50	60	100	99.7[d]	277.8	8
$(Zn_4PMo_{12})_2$	H_2O_2	1.08	50	30	>99	>99	400	9
Cu_6PMo_{12}	TBHP	3.75	40	180	99	100	25.9	10
$Co(PMo_6)_2$	H_2O_2	1.2	rt	20	99.5	98	298.5	11
$Mn(PMo_6)_2$	H_2O_2	1.2	rt	20	96.3	97.1	288.9	11
$Ni(PMo_6)_2$	H_2O_2	1.2	rt	20	98.3	97.6	294.9	11
$Zn(PMo_6)_2$	H_2O_2	1.2	rt	20	97.3	97.4	291.9	11
$CuTeMo_6$	TBHP	1.1	40	60	97	99	1616.7	12
$Cu_3Co_2Mo_{10}$	TBHP	2	40	240	99	100	16.5	13
$Cu_2Co_2Mo_{10}$	TBHP	2	40	240	98.4	95.2	16.4	13
$Cu_3(Co_2Mo_{10})_2$	TBHP	2	40	240	94.8	95.1	15.8	13
$Cu(Co_2Mo_{10})_2$	TBHP	2	40	240	96.7	96.3	16.1	13
$(Ti_7SbW_9)_2$	H_2O_2	2.8	50	60	100	100[d]	1000	14
$Zr_{24}Ge_6W_{56}$	H_2O_2	3	60	60	99	16	99	15
$Zr_8B_2Si_4W_{40}$	H_2O_2	3	80	180	86	78[d]	57.3	16
$Zr_4P_5Sb_6W_{26}$	H_2O_2	2.4	45	60	100	100[d]	1000	17
$AsNi_{16}Si_4W_{36}$	H_2O_2	5	70	120	100	100[d]	250	18
$Ce_2Se_3W_{31}$	H_2O_2	3	40	60	100	100[d]	500	19
$Nd_4Se_4W_{36}$	H_2O_2	3	35	10	100	100[c]	3000	20
$Ru_3As_4W_{42}$	H_2O_2	1.2	40	60	95.1	99	317	21
$Ru_3As_2W_{21}$	H_2O_2	1.2	40	60	68.2	99	227.3	21
$Ru_2As_4W_{40}$	H_2O_2	2.5	50	60	97.4	87	608.8	22
$Ru_2As_4W_{40}$	H_2O_2	2.5	50	60	100	100[d]	625	22
V^{IV}_8	TBHP	33	40	240	100	—	2.8	23
V^{IV}_8	TBHP	0.67	rt	480	90	97.8	33.8	24
$V^{V}_{17}V^{IV}_{12}$	TBHP	2	rt	60	98	91	326.7	25
CoV_2	TBHP	1.5	50	15	98	98	653.3	26
NiV_2	TBHP	1.5	50	15	100	99	666.7	26
CuV_2	H_2O_2	1.1	40	240	98.7	100	7.3	27
NiV_4	H_2O_2	2.5	40	60	100	100[d]	20	28
MnV_{10}	H_2O_2	1.2	50	240	97.5	98.5	7.6	29
Co_2V_4	TBHP	2.5	50	240	99	100	49.5	30
Ni_2V_4	H_2O_2	1.2	45	240	96.8	98.7	6.9	31
Cu_2V_4	H_2O_2	1.2	45	240	98.8	96.5	7.1	31
Co_4V_8	H_2O_2	1.2	45	240	98.2	96.8	7.0	31
Se_4V_{10}	TBHP	3	rt	60	53.8	100	269	32
$NiSe_8V_{20}$	TBHP	3	rt	60	96.4	100	482	33
$Mn_4Se_8V_{20}$	TBHP	3	rt	60	96.3	100	481.5	32

$Co_4Se_8V_{20}$	TBHP	3	rt	60	98.9	100	494.5	32
$Zn_4Se_8V_{20}$	TBHP	3	rt	60	97.9	100	489.5	32
$Mn_6Se_8V_{20}$	TBHP	3	rt	60	96.2	97.8	481	34
$Co_6Se_8V_{20}$	TBHP	3	rt	60	98.8	97.9	494	34
$Zn_6Se_8V_{20}$	TBHP	3	rt	60	96.5	97.8	482.5	34

[a]O/S = the molar ratio of oxidant to substrate. [b]Selectivity to MPSO. [c]Turnover frequency (TOF) = (mol of MPS consumed)/(mol of the catalyst used × reaction time). [c]This work. [d]Selectivity to $MPSO_2$.

Table S5. The effect of solvent on MPS oxidation catalyzed by compound **1**[a].

entry	solvent	con. (%)[b]	sel. (%)[c]	TOF (h^{-1})[d]	TOF (h^{-1})[e]
1	**MeOH**	**>99**	**>99**	**1200**	**1200**
2	EtOH	94.2	97.0	1130.4	1096.5
3	i-PrOH	90.0	>99	1080	1080
4	n-BuOH	96.0	96.3	1152	1109.4
5	Cyclohexanol	>99	96.1	1200	1153.2
6	Acetone	85.0	>99	1020	1020
7	MeCN	86.5	98.0	1038	1017.2
8	DMF	45.7	>99	548.4	548.4
9	DMSO	37.2	>99	446.4	446.4

[a]Reaction conditions: 0.25 mmol of MPS, 0.5 mol% of compound **1**, 1.2 equivalents of H_2O_2, 0.5 mL of solvent, 50 ºC, 10 min. [b]Results determined by GC using naphthalene as internal standard. [c]Selectivity to MPSO. [d]Turnover frequency (TOF) = (mol of MPS consumed)/(mol of the catalyst used × reaction time). [e]Turnover frequency (TOF) = (mol of MPSO generated)/(mol of the catalyst used × reaction time).

Table S6. Formula required for kinetic study.

	k (min^{-1})			E_a (kJ·mol^{-1})	$\Delta H^{\neq}$ (kJ·mol^{-1})	$\Delta S^{\neq}$ (J·mol^{-1}·K^{-1})
	40 ºC	45 ºC	50 ºC			
1	0.1294	0.2160	**0.4493**	95.16	92.47	6.56
2	0.0901	0.1514	**0.2981**	100.64	97.95	20.09

[a]All results are based on the first-order kinetic simulation curve. Except for the rate constant (k), the calculation of other parameters is based on the optimal conditions. The meaning of some variables and constants in the following formulas (the unit or constant value are listed in parentheses). c_0: the initial TMP concentrations (mol·L^{-1}). c_t: the TMP concentration at the specified time (mol·L^{-1}). k: rate constant (min^{-1}). E_a: activation energy (kJ·mol^{-1}). R: gas constant (8.314 J·mol^{-1}·K^{-1}). T: reaction temperature (K). A: preexponential factor. $\Delta H^{\neq}$: activation enthalpy (kJ·mol^{-1}). $\Delta S^{\neq}$: activation entropy (J·mol^{-1}·K^{-1}). k_B: Boltzmann constant (1.38×10^{-23} J·K^{-1}). h: Planck constant (6.62×10^{-34} J·s = 1.10×10^{-35} J·min). $c^{\ominus}$: substrate concentration (mol·L^{-1}). n: order of reaction.

$$ln(\frac{C_t}{C_0}) = -kt \qquad \textbf{Eq. S1}$$

$$lnk = -\frac{E_a}{RT} + lnA \qquad \textbf{Eq. S2}$$

$$\triangle H^{\neq} = E_a - RT \qquad \textbf{Eq. S3}$$

$$k = -\frac{k_a T}{h}(c^{\ominus})^{1-n} exp\left[-\frac{\triangle r^{\neq}H_m(c^{\ominus})}{RT}\right] exp\left[-\frac{\triangle r^{\neq}S_m(c^{\ominus})}{R}\right] \qquad \textbf{Eq. S4}$$

Table S7. Characterization of partially oxidation products catalyzed by compound **1**.

products	m/z	^{1}H NMR (ppm)[a]
methyl phenyl sulfoxide	140(M$^+$), 125, 109, 97, 77, 65, 51	2.64 (s, 3H), 7.49 (m, 2h), 7.53 (m, 1H), 7.54 (d, 2H)
methyl *p*-tolyl sulfoxide	154(M$^+$), 139, 123, 91, 77, 65, 51, 49, 35	2.43 (s, 3H), 2.61 (s, 3H), 7.30 (d, 2H), 7.44 (d, 2H)
4-methoxyphenyl methyl sulfoxide	170(M$^+$), 155, 139, 123, 110, 96, 77, 63	2.66 (s, 3H), 3.82 (s, 3H), 6.99 (d, 2H), 7.56 (d, 2H)
4-bromophenyl methyl sulfoxide	220(HM$^+$), 218, 205, 203, 175, 155, 139, 108, 96	2.67 (s, 3H), 7.48 (d, 2H), 7.62 (d, 2H)
2-pyridyl methyl sulfoxide	141(M$^+$), 124, 93, 78, 51	2.99 (s, 3H), 7.66 (m, 1H), 7.66 (m, 1H), 8.10 (m, 1H), 8.64 (q, 1H)
3-methanesulfinyl-2-methylfuran	144(M$^+$), 116, 85, 59, 45	2.30 (s, 3H), 2.52 (s, 3H), 6.42 (d, 1H), 7.58 (d, 1H)
(phenylsulfinyl)cyclopropane	166(M$^+$), 125, 117, 97, 78, 62	0.81-1.06 (m, 2H), 1.27 (m, 2H), 7.53 (m, 1H), 7.49 (m, 2H), 7.54 (m, 2H)
phenyl sulfoxide	202(M$^+$), 186, 185, 173, 154, 141, 125, 109, 97, 77, 65, 51, 39	7.64 (m, 4H), 7.49 (m, 6H)
dibutyl sulfoxide	162(M$^+$), 146, 106. 88, 61, 56, 41, 29	0.89 (t, 6H), 1.30 (m, 4H), 1.39 (m, 4H), 2.55 (t, 4H)
2-chloroethyl ethyl sulfoxide	124(M$^+$), 75, 61, 47, 29	1.16 (t, 3H), 2.61 (q, 2H), 2.85 (t, 2H), 3.72 (t, 2H)

[a] 400 MHz and DMSO as solvent.

Section V. References

1. T. Sun, J.-P. Ma, R.-Q. Huang and Y.-B. Dong, The inner salt 4-carboxy-2-(pyridinium-4-yl)-1H-imidazole-5-carboxylate monohydrate, *Acta Crystallographica Section E Structure Reports Online*, 2006, **62**, o2751−o2752.
2. E. Alcalde, I. Dinarés, L. Pérez-García and T. Roca, An advantageous synthesis of 2-substituted benzimidazoles using polyphosphoric acid. 2-(pyridyl)-1H-benzimidazoles, 1-alkyl-(1H-benzimidazol-2-yl)pyridinium salts, their homologues and vinylogues, *Synthesis*, 1992, **1992**, 395−398.
3. G. M. Sheldrick, *SHELXS97 and SHELXL97. Program for Crystal Structure Solution and Refinement*, University of Göttingen, Göttingen, Germany, 1997.
4. G. M. Sheldrick, SHELXT-integrated space-group and crystal-structure determination, *Acta Crystallogr., Sect. A: Found. Adv.*, 2015, **71**, 3−8.
5. A. L. Spek, Single-crystal structure validation with the program PLATON, *J. Appl. Crystallogr.*, 2003, **36**, 7−13.
6. A. Rezaeifard, R. Haddad, M. Jafarpour and M. Hakimi, $\{Mo_{132}\}$ nanoball as an efficient and cost-effective catalyst for sustainable oxidation of sulfides and olefins with hydrogen peroxide, *ACS Sustainable Chem. Eng.*, 2014, **2**, 942−950.
7. X. L. Wang, J. Y. Zhang, Z. H. Chang, Z. Zhang, X. Wang, H. Y. Lin and Z. W. Cui, α–γ-Type $[Mo_8O_{26}]^{4-}$ -containing metal–organic complex possessing efficient catalytic activity toward the oxidation of thioether derivatives, *Inorg. Chem.*, 2021, **60**, 3331−3337.
8. J. Wang, Y. Niu, M. Zhang, P. Ma, C. Zhang, J. Niu and J. Wang, Organophosphonate-functionalized lanthanopolyoxomolybdate: synthesis, characterization, magnetism, luminescence, and catalysis of H_2O_2-based thioether oxidation, *Inorg. Chem.*, 2018, **57**, 1796−1805.
9. Y. Chen, S. Chang, H. An, Y. Li, Q. Zhu, H. Luo and Y. Huang, Two polymorphic polyoxometalate-based metal–organic frameworks for the efficient synthesis of functionalized sulfoxides and detoxification of mustard gas simulants, *ACS Sustainable Chem. Eng.*, 2021, **9**, 15683−15693.
10. Y. L. Xiong, M. Y. Yu, T. T. Guo, J. Yang and J. F. Ma, A nanosized propeller-like polyoxometalate-linked copper(I)-resorcin[4]arene for efficient catalysis, *Inorg. Chem.*, 2020, **59**, 15402−15409.
11. H. An, Y. Hou, S. Chang, J. Zhang and Q. Zhu, Highly efficient oxidation of various thioethers catalyzed by organic ligand-modified polyoxomolybdates, *Inorg. Chem. Front.*, 2020, **7**, 169−176.
12. Q. Xu, X. Liang, B. Xu, J. Wang, P. He, P. Ma, J. Feng, J. Wang and J. Niu, 36-Nuclearity organophosphonate-functionalized polyoxomolybdates: synthesis, characterization and selective catalytic oxidation of sulfides, *Chem. Eur. J.*, 2020, **26**, 14896−14902.
13. H. Y. An, Y. J. Hou, L. Wang, Y. M. Zhang, W. Yang and S. Z. Chang, Evans-Showell-type polyoxometalates constructing high-dimensional inorganic-organic hybrid compounds with copper-organic coordination complexes: synthesis and oxidation catalysis, *Inorg. Chem.*, 2017, **56**, 11619−11632.
14. H. L. Li, C. Lian, D. P. Yin, Z.-Y. Jia and G. Y. Yang, A new hepta-nuclear Ti-oxo-cluster-substituted tungstoantimonate and its catalytic oxidation of thioethers, *Cryst. Growth Des.*, 2018, **19**, 376−380.
15. L. Huang, S. S. Wang, J. W. Zhao, L. Cheng and G. Y. Yang, Synergistic combination of multi-Zr(IV) cations and lacunary keggin germanotungstates leading to a gigantic Zr_{24}-cluster-substituted polyoxometalate, *J. Am. Chem. Soc.*, 2014, **136**, 7637−7642.
16. Z. Zhang, Y. L. Wang, Y. Liu, S. L. Huang and G. Y. Yang, Three ring-shaped Zr(IV)-substituted silicotungstates: syntheses, structures and their properties, *Nanoscale*, 2020, **12**, 18333−18341.
17. H. L. Li, C. Lian, D. P. Yin and G. Y. Yang, Three Zr(IV)-substituted polyoxotungstate aggregates: structural transformation from tungstoantimonate to tungstophosphate induced by pH, *Inorg. Chem.*, 2020, **59**, 12842−12849.
18. C. Lian, H. L. Li and G. Y. Yang, A μ-AsO_4-bridging hexadecanuclear Ni-substituted polyoxotungstate, *Inorg. Chem.*, 2021, **60**, 3996-4003.
19. H. L. Li, C. Lian, L. J. Chen, J. W. Zhao and G. Y. Yang, Two Ce^{3+}-Substituted selenotungstates regulated by N, N-dimethylethanolamine and dimethylamine hydrochloride, *Inorg. Chem.*, 2019, **58**, 8442−8450.

20. H. Li, C. Lian, L. Chen, J. Zhao and G. Y. Yang, Two unusual nanosized Nd^{3+}-substituted selenotungstate aggregates simultaneously comprising lacunary Keggin and Dawson polyoxotungstate segments, *Nanoscale*, 2020, **12**, 16091−16101.

21. H. Li, P. He, R. Wan, Y. Zou, X. Zhao, P. Ma, J. Niu and J. Wang, Trinuclear ruthenium core-containing polyoxometalate-based hybrids: preparation, characterization and catalytic behavior, *Dalton Trans.*, 2020, **49**, 2895−2904.

22. M. Han, Y. Niu, R. Wan, Q. Xu, J. Lu, P. Ma, C. Zhang, J. Niu and J. Wang, A crown-shaped Ru-Substituted arsenotungstate for selective oxidation of sulfides with hydrogen peroxide, *Chem. Eur. J.*, 2018, **24**, 11059−11066.

23. J. P. Cao, Y. S. Xue, N. F. Li, J. J. Gong, R. K. Kang and Y. Xu, Lewis acid dominant windmill-shaped V_8 clusters: a bifunctional heterogeneous catalyst for CO_2 cycloaddition and oxidation of sulfides, *J. Am. Chem. Soc.*, 2019, **141**, 19487−19497.

24. J. Tang, P. F. Yao, X. L. Xu, H. Y. Li, F. P. Huang, Q.-Q. Nie, M. Y. Luo, Q. Yu and H. D. Bian, Asymmetric catalytic sulfoxidation by a novel $V^{IV}{}_8$ cluster catalyst in the presence of serum albumin: a simple and green oxidation system, *RSC Adv.*, 2016, **6**, 44154−44162.

25. K. Wang, Y. Niu, D. Zhao, Y. Zhao, P. Ma, D. Zhang, J. Wang and J. Niu, The polyoxovanadate-based carboxylate derivative $K_6H[V^V{}_{17}V^{IV}{}_{12}(OH)_4O_{60}(OOC(CH_2)_4COO)_8]\cdot nH_2O$: synthesis, crystal structure, and catalysis for oxidation of sulfides, *Inorg. Chem.*, 2017, **56**, 14053−14059.

26. X. Wang, T. Zhang, Y. H. Li, J. F. Lin, H. Li and X. L. Wang, In situ ligand-transformation-involved synthesis of inorganic-organic hybrid polyoxovanadates as efficient heterogeneous catalysts for the selective oxidation of sulfides, *Inorg. Chem.*, 2020, **59**, 17583−17590.

27. J. Li, X. Huang, S. Yang, Y. Xu and C. Hu, Controllable synthesis, characterization, and catalytic properties of three inorganic–organic hybrid copper vanadates in the highly selective oxidation of sulfides and alcohols, *Cryst. Growth Des.*, 2015, **15**, 1907−1914.

28. T. Y. Dang, R.-H. Li, H. R. Tian, Q. Wang, Y. Lu and S. X. Liu, Tandem-like vanadium cluster chains in a polyoxovanadate-based metal–organic framework for efficient catalytic oxidation of sulfides, *Inorg. Chem. Front.*, 2021, **8**, 4367−4375.

29. J. K. Li, C. P. Wei, Y. Y. Wang, M. Zhang, X. R. Lv and C. W. Hu, Conversion of V_6 To V_{10} cluster: decavanadate-based Mn-polyoxovanadate as robust heterogeneous catalyst for sulfoxidation of sulfides, *Inorg. Chem. Commun.*, 2018, **87**, 5−7.

30. B. B. Lu, J. Yang, Y. Y. Liu and J. F. Ma, A polyoxovanadate-resorcin[4]arene-based porous metal-organic framework as an efficient multifunctional catalyst for the cycloaddition of CO_2 with epoxides and the selective oxidation of sulfides, *Inorg. Chem.*, 2017, **59**, 11710−11720.

31. J. Li, C. Wei, D. Guo, C. Wang, Y. Han, G. He, J. Zhang, X. Huang and C. Hu, Inorganic-organic hybrid polyoxovanadates based on $[V_4O_{12}]^{4-}$ or $[VO_3]^{22-}$ clusters: controllable synthesis, crystal structures and catalytic properties in selective oxidation of sulfides, *Dalton Trans.*, 2020, **49**, 14148−14157.

32. R. Wan, P. He, Z. Liu, X. Ma, P. Ma, V. Singh, C. Zhang, J. Niu and J. Wang, A lacunary polyoxovanadate precursor and transition-metal-sandwiched derivatives for catalytic oxidation of sulfides, *Chem. Eur. J.*, 2020, **26**, 8760−8766.

33. J. P. Liu, Z. H. Deng, Q. Xu, R. Wan, P. T. Ma, J. Y. Niu and J. P. Wang, Synthesis, structure and catalytic study of a new sandwiched-type vanadoselenite, *Inorg. Chem. Commun.*, 2021, **124**, 108407−108410.

34. R. Wan, Z. Jing, Q. Xu, X. Ma, P. Ma, C. Zhang, J. Niu and J. Wang, Lacunary $\{Se_4V_{10}\}$ heteropolyoxovanadate precursor with monometal, metal-richer-sandwiched dedrivatives $\{Se_8V_{20}M\}$ and $\{Se_8V_{20}M_3\}$: correlations between the synthesis, structure, and catalytic property, *Inorg. Chem.*, 2021, **60**, 2888−2892.